JACS
JOURNAL OF THE AMERICAN CHEMICAL SOCIETY
pubs.acs.org/JACS
Article

Chirality-Induced Magnetoresistance Due to Thermally Driven Spin Polarization

Kouta Kondou,*,# Masanobu Shiga,# Shoya Sakamoto, Hiroyuki Inuzuka, Atsuko Nihonyanagi, Fumito Araoka, Masaki Kobayashi, Shinji Miwa,* Daigo Miyajima, and YoshiChika Otani

Cite This: J. Am. Chem. Soc. 2022, 144, 7302−7307
Read Online
ACCESS | Metrics & More | Article Recommendations | Supporting Information

ABSTRACT: Chirality-induced current-perpendicular-to-plane magnetoresistance (CPP-MR) originates from current-induced spin polarization in molecules. The current-induced spin polarization is widely recognized as a fundamental principle of chiral-induced spin selectivity (CISS). In this study, we investigate chirality-induced current-in-plane magnetoresistance (CIP-MR) in a chiral molecule/ferromagnetic metal bilayer at room temperature. In contrast to CPP-MR, CIP-MR observed in the present study requires no bias charge current through the molecule. The temperature dependence of CIP-MR suggests that thermally driven spontaneous spin polarization in chiral molecules is the key to the observed MR. The novel MR is consistent with recent CISS-related studies, that is, chiral molecules in contact with a metallic surface possess a finite spin polarization.

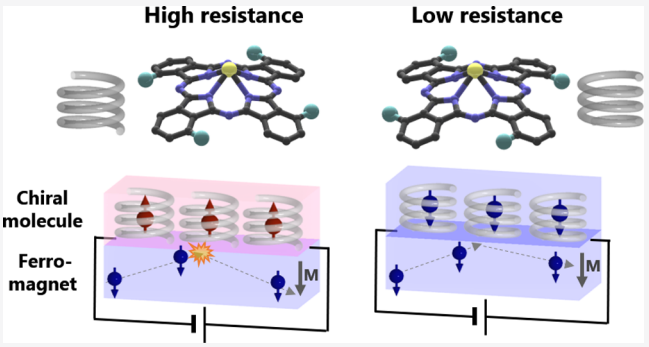

INTRODUCTION

Molecular chirality is an essential factor in the induction of spin functionalities in organic materials. The spin polarization of electrons passing through chiral molecules has been extensively investigated for 2 decades.[1−18] This property is called the chiral-induced spin selectivity (CISS) effect, which has been confirmed using various experimental techniques such as photoelectron spectroscopy,[3,11] current-perpendicular-to-plane (CPP) magnetoresistance (MR) measurements,[7,8,14] spin-polarized conductive atomic force microscopy,[4,10,12,14,19,20] Hall voltage detection,[15,21] and magnetization control.[22,23] Surprisingly, a large spin polarization that is comparable to that of ferromagnets appears at room temperature despite the weak spin−orbit coupling of light elements in such chiral molecules.[3,6,9,10,12−14] The physical origins of chirality-induced large spin polarization[2,5,24−30] and related phenomena such as two-terminal MR[31,32] remain elusive. Nevertheless, such chirality-induced phenomena can be applied to nanoscale spin manipulation in spintronics, quantum computing, and biochemistry.

True and false chiralities have been defined by Barron in 1986.[33] According to this definition, a translating spinning cone is truly chiral, whereas a non-translating, that is, stationary spinning cone is not. This statement helps to understand chirality-induced phenomena such as nonreciprocal transport in various chiral systems.[34,35] In the case of chirality-induced current-perpendicular-to-plane magnetoresistance (CPP-MR) in a chiral molecule/ferromagnet system, the current-induced spin polarization in the chiral molecule is the translating spinning cone that gives rise to the MR.

However, several experimental studies have recently reported that chiral molecules behave like magnets.[22,36−39] For instance, a chiral molecule adsorbed on a superconductor surface exhibits in-gap states similar to the magnetic impurity-induced state in the tunneling spectra.[36] Moreover, a chirality-dependent effective magnetic field is generated in the ferromagnetic metal/chiral molecule bilayer.[22,37] Remarkably, no bias charge current flows through the molecule, implying that magnetization, that is, spontaneous spin polarization, may emerge in the chiral molecules. However, chirality-dependent spontaneous spin polarization cannot occur in the ground state because the spin polarization itself is falsely chiral.[33] Therefore, these experimental results should be understood differently from steady[1,2,4−16,19−21] or transient[22,23] current-induced spin polarization, which is widely recognized as a fundamental principle of CISS. To explain the spontaneous spin polarization in chiral molecules indicated by recent CISS-related experimental studies,[22,36−39] one should consider a thermally driven

Received: January 16, 2022
Published: April 13, 2022

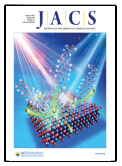

https://doi.org/10.1021/jacs.2c00496
J. Am. Chem. Soc. 2022, 144, 7302−7307

microscopic flow of spin angular momentum to make the system truly chiral.

Recently, it has been proposed that when a chiral molecule is in contact with a metallic surface, molecular vibrations induce charge redistribution and spontaneous spin polarization.[40] In this study, we have experimentally demonstrated CISS-related spontaneous spin polarization using MR measurements.

RESULTS

Concept of Chiral-Molecule-Induced Current-in-Plane Magnetoresistance. This paper reports the first observation of the current-in-plane magnetoresistance (CIP-MR) effect at room temperature in a chiral molecule/ferromagnet bilayer system. In general, the MR effect appears in ferromagnetic metal/non-magnetic metal/ferromagnetic metal multilayer systems. Figure 1a shows a schematic of the current-in-plane giant magnetoresistance (CIP-GMR) effect. The overall electrical resistance varies with the change in the spin-dependent electron scattering owing to the shift in the chemical potential at the interface[41−44] and is dependent on the relative direction of magnetization in the two ferromagnetic layers. Similarly, we investigated the chirality-induced CIP-MR effect using the chiral molecule/ferromagnetic heterostructure shown in Figure 1b. The CIP-MR shown in Figure 1b reflects the spontaneous spin polarization emerging in a chiral molecule via spin-dependent scattering. Note that the device configuration in this study is essentially different from the previously reported CPP-MR, in which a bias voltage is applied through the molecule/ferromagnet interface, and the charge current in the molecule flows parallel to the magnetization switching direction in the ferromagnet.[4,7,8,10,12,14,16,19,20] In our CIP-MR devices, a bias voltage is applied along the wire, and most of the charge current flows through the ferromagnetic metal (Ni in this work) because the electrical conductivity of the molecule is approximately 15 orders of magnitude smaller than that of the ferromagnet.[45] Moreover, the direction of the current-induced spin polarization in the molecule is normal to that of the magnetization switching of the ferromagnet, which does not contribute to the MR. Therefore, the CIP-MR configuration is suitable for detecting the CISS-related spontaneous spin polarization in a chiral molecule without being affected by the current-induced spin polarization.

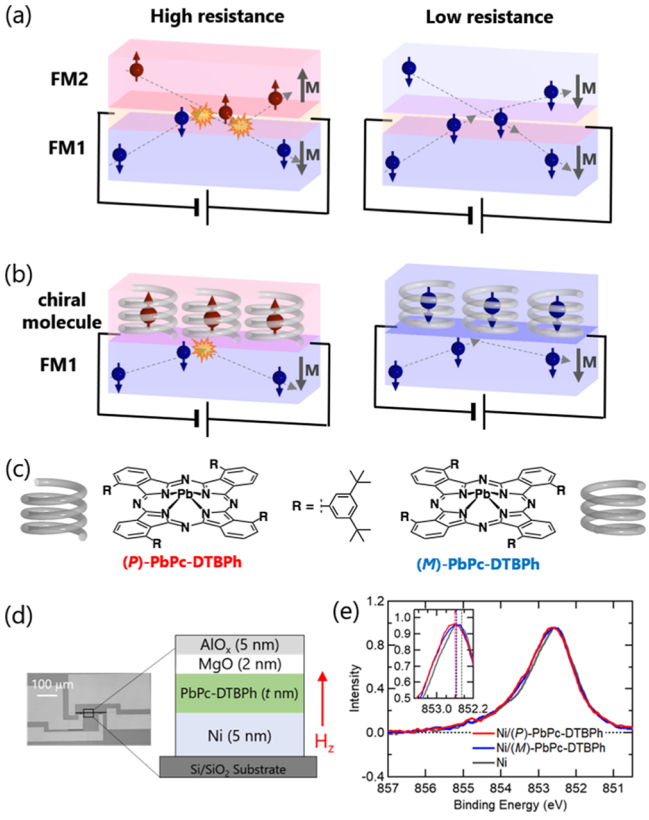

Figure 1. Concept of chiral-molecule-induced current-in-plane MR. (a,b) Schematic illustration of a conventional metal-based CIP-GMR effect and a chiral-molecule-induced MR effect. Springs beside each chiral molecule denote the helicity. (c) Structure of the chiral molecule. Right-handed helicity: (*P*)-PbPc-DTBPh and left-handed helicity: (*M*)-PbPc-DTBPh. (d) Scanning electron micrograph of a measurement sample and schematic of the multilayer. (e) XPS spectrum in Ni/PbPc-DTBPh films.

In this study, we employed chiral molecules of (*P*)- and (*M*)-PbPc-DTBPh, as shown in Figure 1c, which have right- and left-handed helicities, respectively. The detailed synthesis methods have been reported in the literature.[37] Figure 1d shows the scanning electron microscopy image and a schematic illustration of the measured multilayer, Ni(5 nm)/(*P*)- or (*M*)-PbPc-DTBPh(0−1 nm)/MgO(2 nm)/AlO_x(5 nm), on a thermally oxidized Si substrate. The PbPc-DTBPh layer was deposited at an evaporation rate of 5×10^{-3} nm s^{-1} (0.05 Å s^{-1}) in ultrahigh vacuum (<5×10^{-7} Pa). The molecular thickness was determined using a quartz thickness monitor equipped with a vacuum chamber. Each molecular layer of PbPc-DTBPh was approximately 0.6 nm. The Ni and oxide capping layers of MgO/AlO_x were grown at an evaporation rate of 1×10^{-2} nm s^{-1} (0.1 Å s^{-1}) using electron beam deposition in an ultra-high vacuum (<3×10^{-7} Pa). The molecular orientation does not affect the molecular chirality of PbPc-DTBPh because of its structurally determined nature.[14,37] The Ni/PbPc-DTBPh multilayer films were patterned into 5 μm × 100 μm rectangular shapes using photolithography and Ar-ion milling. The sample resistance was measured using the conventional four-terminal method to remove contact resistance.

Figure 1e shows the X-ray photoemission spectroscopy (XPS) spectrum of the Ni 2*p* core level in Ni/PbPc-DTBPh measured at room temperature. Compared with the control sample of Ni/MgO, we found charge transfer (CT) in which Ni was doped with an electron from PbPc-DTBPh regardless of its chirality. This implies that a hybridized interface state (HIS) appears between the ferromagnetic conduction band and the highest occupied molecular orbital (HOMO) of the chiral molecule[46−48] because there is a high and narrow density of state (DOS) peak in the vicinity of the Fermi level of Ni.

CIP-MR in a Ferromagnet/Chiral Molecule Bilayer System. Figure 2 shows the typical MR curves for the Ni/(*P*)-PbPc-DTBPh-, Ni-, and Ni/(*M*)-PbPc-DTBPh-based multilayers. A Ni sample without the PbPc-DTBPh molecule served as the control sample. The overall sample resistance of the Ni/PbPc-DTBPh bilayer device was slightly larger than that of the control sample. The direction of the applied external magnetic field (H_z) is normal to the film plane. The direct current applied for resistance measurement was 50 μA. Measurements were performed at room temperature. All the sample resistances shown in Figure 2a−c indicate the typical anisotropic MR effect of the Ni layer as the direction of

https://doi.org/10.1021/jacs.2c00496
J. Am. Chem. Soc. 2022, 144, 7302−7307

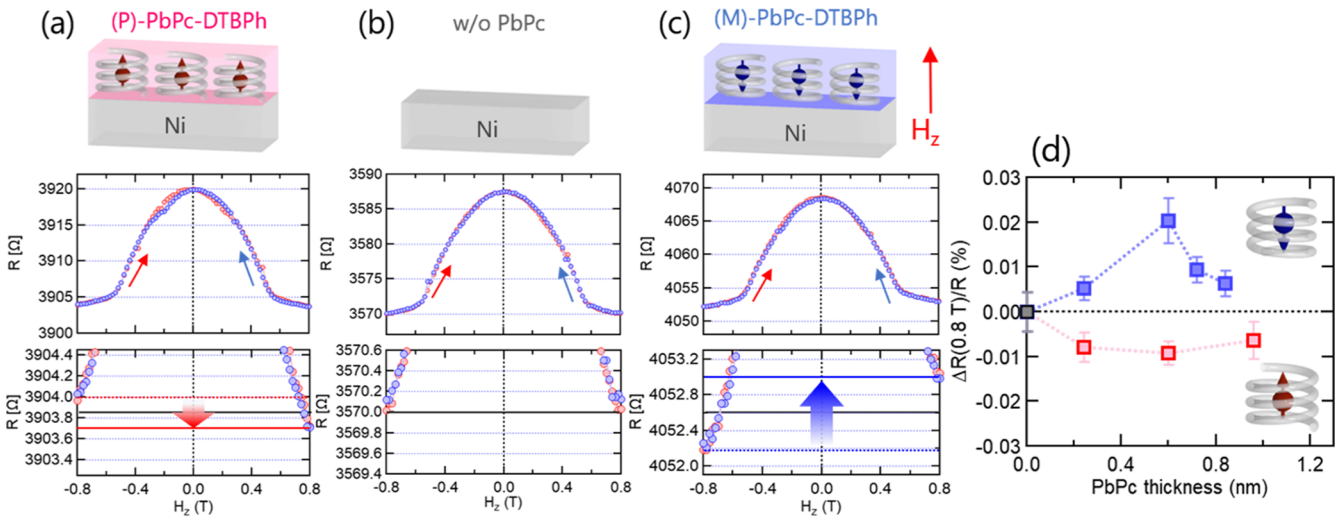

Figure 2. Molecular chirality and thickness dependence. MR measurement in a (a) Ni/(*P*)-PbPc-DTBPh (0.6 nm) film, a (b) Ni film as a control sample, and a (c) Ni/(*M*)-PbPc-DTBPh (0.6 nm) film. Blue and pink open plots correspond to the experimental data in each magnetic field sweep direction shown by red and blue arrows. (d) Molecular thickness dependence of the MR ratio $\Delta R/R$ due to the chiral-molecule-induced CIP-MR effect at room temperature. Red, black, and blue plots correspond to the data in (*P*)-PbPc-DTBPh, the control sample, and (*M*)-PbPc-DTBPh, respectively.

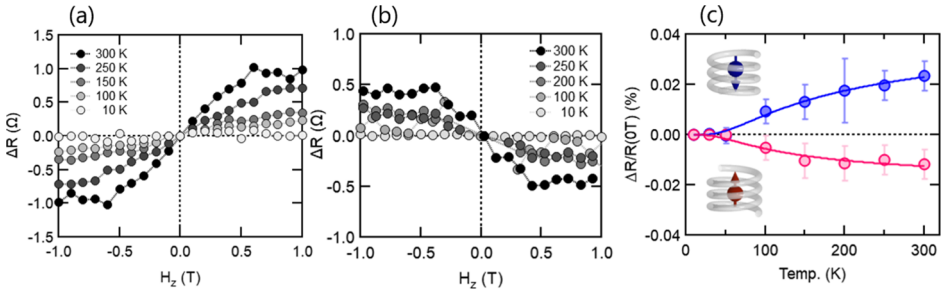

Figure 3. Temperature dependence. Variation of the chirality-induced CIP-MR effect ΔR in a (a) Ni/(*M*)-PbPc-PbPc-DTBPh (0.6 nm) film and (b) Ni/(*P*)-PbPc-PbPc-DTBPh (0.6 nm) as a function of the applied magnetic field at various temperatures. The applied direct current is 10 μA (c) $\Delta R/R$ as a function of the measurement temperature, in which blue and red plots correspond to data for Ni/(*M*)-PbPc-PbPc-DTBPh and Ni/(*P*)-PbPc-PbPc-DTBPh, respectively. The blue and red colored lines are the fitting curves by the Boltzmann distribution function.

magnetization of the Ni layer gradually rotates from in-plane to out-of-plane with the applied H_z field. The MR values in the positive and negative saturation magnetic fields were almost the same as in the control sample. Thus, the surface-roughness-induced GMR effect in the Ni layer was negligible in the sample under study. In the Ni/(*P*)-PbPc-DTBPh bilayer sample, the MR value at the positive saturation magnetic field was smaller than that at the negative saturation magnetic field, as shown in Figure 2a. Most interestingly, in the case of the opposite helicity in the molecule, that is, the Ni/(*M*)-PbPc-DTBPh bilayer shown in Figure 2c, the tendency is reversed; the value at the positive saturation magnetic field is larger than that at the negative saturation magnetic field. The change in MR is independent of the sweep direction of the magnetic field and the probe current amplitude from −100 to +100 μA (Supporting Information), implying that the MR change is not related to the hysteretic magnetic domain formation in the Ni layer and Joule heating by the applied current.

Hence, this must be a chirality-induced CIP-MR effect. These results suggest that the CIP-MR may originate from the spin-dependent scattering at the Ni/chiral molecule interface. The results obtained without being affected by the current-induced spin polarization strongly suggest that the chirality-dependent spontaneous spin polarization emerges inside the molecules, as shown by the red and blue arrows in the schematic illustrations in Figure 2a,c. The above facts are also supported by the recent experimental report on the chirality-induced effective magnetic field in the Fe/PbPc-DTBPh/MgO multilayer.[37] The spin polarization induced in PbPc-DTBPh corresponds to the direction of exchange-coupled magnetization observed in the Fe/PbPc-DTBPh/MgO trilayer.

Figure 2d shows the MR ratio $\Delta R(0.8\ \mathrm{T})/R(0\ \mathrm{T}) \times 100$ (%) with $\Delta R(0.8\ \mathrm{T}) = R(+0.8\ \mathrm{T}) - R(-0.8\ \mathrm{T})$ as a function of molecular thickness up to 1 nm. $R(\pm 0.8\ \mathrm{T})$ and $R(0\ \mathrm{T})$ are the sample resistances at $H_z = \pm 0.8$ and 0 T, respectively. The blue and red squares shown in Figure 2d correspond to the MR ratios of (*M*)-PbPc-DTBPh and (*P*)-PbPc-DTBPh, respectively. The error bars represent the standard deviation of five measurement cycles. The main source of noise is the measurement system, such as a slight instability in the voltage source. With an increase in the amount of molecular adsorption on the Ni layer surface up to ∼0.6 nm (∼one molecular layer: 1 ML), the values of ΔR for both (*M*)- and (*P*)-PbPc-DTBPh increased gradually. This result indicates that the molecular adsorption on the ferromagnetic layer surface causes the MR effect. In contrast, above ∼0.6 nm (1 ML), the values of ΔR for (*M*)- and (*P*)-molecules

https://doi.org/10.1021/jacs.2c00496
J. Am. Chem. Soc. 2022, 144, 7302−7307

considerably decreased with PbPc-DTBPh thickness. This trend is similar to the Rashba interface formation, which results in an increase in the amount of adsorbent achiral PbPc molecules on the Cu surface.[49] According to the study of ref 49, the deformed PbPc stacking caused a significant decline in the spin-to-charge conversion signal above ~1 ML of PbPc on the Cu surface. The XPS spectra shown in Figure 1e indicate a CT between the chiral molecules and the Ni layers. Therefore, the observed dependence on molecular thickness suggests that the HIS at the Ni/PbPc-DTBPh interface plays a crucial role in the emergence of chirality-induced CIP-MR. The difference in the MR ratios of (*P*)-PbPc-PbPc-DTBPh and (*M*)-PbPc-PbPc-DTBPh may originate from the slight inhomogeneity of the molecular film.

DISCUSSION

Temperature Dependence. Here, we discuss the mechanism of the chirality-induced CIP-MR effect, that is, the manner in which spontaneous spin polarization can occur in the chiral molecule. Figure 3a,b shows the resistance change ΔR at various temperatures from 300 to 10 K for the Ni/(*M*,*P*)-PbPc-DTBPh (0.6 nm ~1 ML) bilayer device. To eliminate the anisotropic MR contribution of the Ni layer, we plotted the resistance change ΔR, defined as $\Delta R(\pm H_z) = R(\pm H_z) - R(\mp H_z)$, where $R(\pm H_z)$ is the sample resistance at the positive and negative saturation magnetic fields, respectively. ΔR saturates at around ±0.5 T, which corresponds to the saturation field of the Ni layer. A decrease in temperature from 300 K diminishes the effect, causing ΔR to be almost zero below approximately 50 K. Similarly, the MR ratio defined as $\Delta R(1\ \mathrm{T})/R(0\ \mathrm{T}) \times 100\ (\%)$, shown in Figure 3c, exhibits a gradual decrease and is almost zero below approximately 50 K. This suggests that there is an occurrence of thermally driven spin polarization of the chiral molecules on the Ni layer. By fitting the data to the Boltzmann distribution function $\exp(-\Delta/k_B T)$, where Δ, k_B, and T are the barrier height, the Boltzmann constant, and the temperature, respectively, Δ was estimated to be ~10 meV. This small energy difference may indicate the existence of a HIS at the Ni/PbPc-DTBPh interface.

A possible mechanism for the generation of thermally driven spin polarization in a chiral molecule is shown schematically in Figure 4. Thermally excited hopping charge transport may occur between the conduction band of the metal and the HOMO of the chiral molecule, and the hopping rate increases with temperature. When an electron moves from a metal to a chiral molecule, the electron can be spin-polarized along the out-of-plane (+*z*-direction), assuming that current-induced spin polarization[2,8,12,50−52] occurs during electron transport in the HIS, as indicated by the red arrow. Simultaneously, an electron moves from a chiral molecule to a metal with an opposite spin polarization. We assume that the spin relaxation time in the molecule τ_S^{mol} is longer than the transit time τ_S^t between the metal and the chiral molecule. Here, the spin relaxation time in the metal τ_S^{met}[53] is several orders smaller than τ_S^{mol},[54−56] and the net spin polarization in the system would remain inside the chiral molecule. In this mechanism, the metal layer does not need to be a ferromagnet to generate spin polarization in a chiral molecule. A finite CIP-MR was also observed in the sample, where a thin Cu layer was inserted between Ni and PbPc-DTBPh (Supporting Information). This thermally driven spin polarization explains the temperature dependence of the chirality-induced CIP-MR effect, as shown in Figure 3c. Previous studies on two-terminal CPP-MR have also shown that the MR ratio diminishes with decreasing temperature.[8,10] Thus, thermally induced spin polarization in the chiral molecule may cause a decline in the MR ratio at low temperatures.

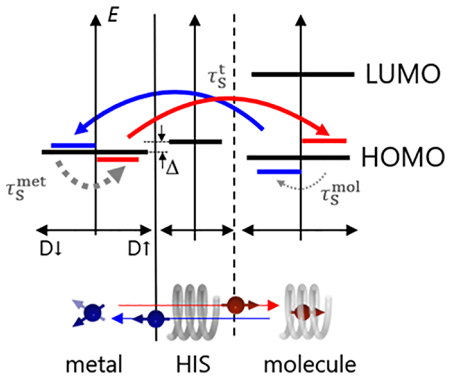

Figure 4. Schematic illustration of thermally driven spin polarization due to charge transport at the metal and the chiral molecule interface. Red and blue bending arrows denote thermally excited electron transport from the metal to the molecule and the molecule to the metal, respectively, that is, thermally excited spin-selective transport. Blue and red lines represent the spin-up DOS D↓ and the spin-down DOS D↑. $\tau_S^{met(mol)}$ and τ_S^t are the spin relaxation time in the metal (molecule) and the transport time between the metal and the molecule.

Indeed, a recent theoretical study pointed out that electron−phonon coupling enhances the current-induced CISS effect.[57,58] Moreover, in a chiral molecule, molecular vibration gives rise to charge redistribution, and a finite spontaneous spin polarization emerges in the molecule when interfaced with a metal.[40] The model assumptions in ref 40 are partially different from ours illustrated in Figure 4, and we believe that the aforementioned mechanism shares the essence with the theory in ref 40.

CONCLUSIONS

In summary, we demonstrated chiral-molecule-induced CIP-MR owing to CISS-related thermally driven, spontaneous spin polarization. In contrast to CPP-MR due to current-induced spin polarization, MR does not require a bias charge current in the chiral molecule. These results indicate the emergence of spin polarization inside the chiral molecules. We believe that thermally driven spin polarization due to spin-selective transport and different spin relaxation times between the metal and chiral molecules is crucial for the emergence of the MR effect. While the MR ratio in the present work is relatively small, a system with all-metallic transport may possess a superior signal-to-noise ratio, which makes it a highly sensitive sensor for biomolecule applications. Our findings could trigger the dramatic development of molecular spintronics, specifically for various types of CISS-related phenomena..

ASSOCIATED CONTENT

Supporting Information

The Supporting Information is available free of charge at https://pubs.acs.org/doi/10.1021/jacs.2c00496.

The Supporting Information is available free of charge on the ACS Publications website. Experimental details and data (PDF)

https://doi.org/10.1021/jacs.2c00496
J. Am. Chem. Soc. 2022, 144, 7302−7307

AUTHOR INFORMATION

Corresponding Authors

Kouta Kondou − *Center for Emergent Matter Science (CEMS), RIKEN, Hirosawa, Wako, Saitama 351-0198, Japan;* orcid.org/0000-0002-3020-3189; Email: kkondou@riken.jp

Shinji Miwa − *The Institute for Solid State Physics, The University of Tokyo, Kashiwa, Chiba 277-8581, Japan; Center for Spintronics Research Network (CSRN), The University of Tokyo, Tokyo 113-8656, Japan; Trans-scale Quantum Science Institute, The University of Tokyo, Tokyo 113-0033, Japan;* orcid.org/0000-0001-9131-6753; Email: miwa@issp.u-tokyo.ac.jp

Authors

Masanobu Shiga − *The Institute for Solid State Physics, The University of Tokyo, Kashiwa, Chiba 277-8581, Japan*

Shoya Sakamoto − *The Institute for Solid State Physics, The University of Tokyo, Kashiwa, Chiba 277-8581, Japan;* orcid.org/0000-0002-2405-1465

Hiroyuki Inuzuka − *Center for Emergent Matter Science (CEMS), RIKEN, Hirosawa, Wako, Saitama 351-0198, Japan*

Atsuko Nihonyanagi − *Center for Emergent Matter Science (CEMS), RIKEN, Hirosawa, Wako, Saitama 351-0198, Japan*

Fumito Araoka − *Center for Emergent Matter Science (CEMS), RIKEN, Hirosawa, Wako, Saitama 351-0198, Japan;* orcid.org/0000-0002-9387-6081

Masaki Kobayashi − *Department of Electrical Engineering and Information Systems and Center for Spintronics Research Network (CSRN), The University of Tokyo, Tokyo 113-8656, Japan*

Daigo Miyajima − *Center for Emergent Matter Science (CEMS), RIKEN, Hirosawa, Wako, Saitama 351-0198, Japan;* orcid.org/0000-0002-9578-7349

YoshiChika Otani − *Center for Emergent Matter Science (CEMS), RIKEN, Hirosawa, Wako, Saitama 351-0198, Japan; The Institute for Solid State Physics, The University of Tokyo, Kashiwa, Chiba 277-8581, Japan; Center for Spintronics Research Network (CSRN), The University of Tokyo, Tokyo 113-8656, Japan; Trans-scale Quantum Science Institute, The University of Tokyo, Tokyo 113-0033, Japan*

Complete contact information is available at: https://pubs.acs.org/10.1021/jacs.2c00496

Author Contributions

#K.K. and M.S. contributed equally to this study.

Notes

The authors declare no competing financial interest.

ACKNOWLEDGMENTS

We thank E. Minamitani, A. Shitade, and M. Haze for fruitful discussions. This work was supported by JSPS-KAKENHI (18H03880 and 19H02586). This work was partially supported by the Spintronics Research Network of Japan (Spin-RNJ).

REFERENCES

(1) Ray, K.; Ananthavel, S. P.; Waldeck, D. H.; Naaman, R. Asymmetric scattering of polarized electrons by organized organic films of chiral molecules. *Science* **1999**, *283*, 814−816.

(2) Yeganeh, S.; Ratner, M. A.; Medina, E.; Mujica, V. Chiral electron transport: scattering through helical potentials. *J. Chem. Phys.* **2009**, *131*, 014707.

(3) Göhler, B.; Hamelbeck, V.; Markus, T. Z.; Kettner, M.; Hanne, G. F.; Vager, Z.; Naaman, R.; Zacharias, H. Spin selectivity in electron transmission through self-assembled monolayers of double-stranded DNA. *Science* **2011**, *331*, 894−897.

(4) Xie, Z.; Markus, T. Z.; Cohen, S. R.; Vager, Z.; Gutierrez, R.; Naaman, R. Spin specific electron conduction through DNA oligomers. *Nano Lett.* **2011**, *11*, 4652−4655.

(5) Guo, A.-M.; Sun, Q.-f. Spin-selective transport of electrons in DNA double helix. *Phys. Rev. Lett.* **2012**, *108*, 218102.

(6) Naaman, R.; Waldeck, D. H. Chiral-Induced Spin Selectivity Effect. *J. Phys. Chem. Lett.* **2012**, *3*, 2178−2187.

(7) Senthil Kumar, K.; Kantor-Uriel, N.; Mathew, S. P.; Guliamov, R.; Naaman, R. A device for measuring spin selectivity in electron transfer. *Phys. Chem. Chem. Phys.* **2013**, *15*, 18357−18362.

(8) Mondal, P. C.; Kantor-Uriel, N.; Mathew, S. P.; Tassinari, F.; Fontanesi, C.; Naaman, R. Chiral conductive polymers as spin filters. *Adv. Mater.* **2015**, *27*, 1924−1927.

(9) Naaman, R.; Waldeck, D. H. Spintronics and chirality: spin selectivity in electron transport through chiral molecules. *Annu. Rev. Phys. Chem.* **2015**, *66*, 263−281.

(10) Kiran, V.; Mathew, S. P.; Cohen, S. R.; Hernández Delgado, I.; Lacour, J.; Naaman, R. Helicenes–A New Class of Organic Spin Filter. *Adv. Mater.* **2016**, *28*, 1957−1962.

(11) Kettner, M.; Maslyuk, V. V.; Nürenberg, D.; Seibel, J.; Gutierrez, R.; Cuniberti, G.; Ernst, K.-H.; Zacharias, H. Chirality-Dependent Electron Spin Filtering by Molecular Monolayers of Helicenes. *J. Phys. Chem. Lett.* **2018**, *9*, 2025−2030.

(12) Tassinari, F.; Jayarathna, D. R.; Kantor-Uriel, N.; Davis, K. L.; Varade, V.; Achim, C.; Naaman, R. Chirality Dependent Charge Transfer Rate in Oligopeptides. *Adv. Mater.* **2018**, *30*, No. e1706423.

(13) Naaman, R.; Paltiel, Y.; Waldeck, D. H. Chiral molecules and the electron spin. *Nat. Rev. Chem.* **2019**, *3*, 250−260.

(14) Suda, M.; Thathong, Y.; Promarak, V.; Kojima, H.; Nakamura, M.; Shiraogawa, T.; Ehara, M.; Yamamoto, H. M. Light-driven molecular switch for reconfigurable spin filters. *Nat. Commun.* **2019**, *10*, 2455.

(15) Inui, A.; Aoki, R.; Nishiue, Y.; Shiota, K.; Kousaka, Y.; Shishido, H.; Hirobe, D.; Suda, M.; Ohe, J.-i.; Kishine, J.-i.; Yamamoto, H. M.; Togawa, Y. Chirality-Induced Spin-Polarized State of a Chiral Crystal $CrNb_3S_6$. *Phys. Rev. Lett.* **2020**, *124*, 166602.

(16) Torres-Cavanillas, R.; Escorcia-Ariza, G.; Brotons-Alcázar, I.; Sanchis-Gual, R.; Mondal, P. C.; Rosaleny, L. E.; Giménez-Santamarina, S.; Sessolo, M.; Galbiati, M.; Tatay, S.; Gaita-Ariño, A.; Forment-Aliaga, A.; Cardona-Serra, S. Reinforced Room-Temperature Spin Filtering in Chiral Paramagnetic Metallopeptides. *J. Am. Chem. Soc.* **2020**, *142*, 17572−17580.

(17) Alwan, S.; Dubi, Y. Spinterface Origin for the Chirality-Induced Spin-Selectivity Effect. *J. Am. Chem. Soc.* **2021**, *143*, 14235−14241.

(18) Huisman, K. H.; Thijssen, J. M. CISS Effect: A Magneto-resistance Through Inelastic Scattering. *J. Phys. Chem. C* **2021**, *125*, 23364−23369.

(19) Kulkarni, C.; Mondal, A. K.; Das, T. K.; Grinbom, G.; Tassinari, F.; Mabesoone, M. F. J.; Meijer, E. W.; Naaman, R. Highly Efficient and Tunable Filtering of Electrons' Spin by Supramolecular Chirality of Nanofiber-Based Materials. *Adv. Mater.* **2020**, *32*, No. e1904965.

(20) Mishra, S.; Mondal, A. K.; Smolinsky, E. Z. B.; Naaman, R.; Maeda, K.; Nishimura, T.; Taniguchi, T.; Yoshida, T.; Takayama, K.; Yashima, E. Spin Filtering Along Chiral Polymers. *Angew. Chem., Int. Ed. Engl.* **2020**, *59*, 14671−14676.

(21) Kumar, A.; Capua, E.; Kesharwani, M. K.; Martin, J. M. L.; Sitbon, E.; Waldeck, D. H.; Naaman, R. Chirality-induced spin

polarization places symmetry constraints on biomolecular interactions. *Proc. Natl. Acad. Sci. U.S.A.* **2017**, *114*, 2474−2478.
(22) Ben Dor, O.; Yochelis, S.; Radko, A.; Vankayala, K.; Capua, E.; Capua, A.; Yang, S.-H.; Baczewski, L. T.; Parkin, S. S. P.; Naaman, R.; Paltiel, Y. Magnetization switching in ferromagnets by adsorbed chiral molecules without current or external magnetic field. *Nat. Commun.* **2017**, *8*, 14567.
(23) Meirzada, I.; Sukenik, N.; Haim, G.; Yochelis, S.; Baczewski, L. T.; Paltiel, Y.; Bar-Gill, N. Long-Time-Scale Magnetization Ordering Induced by an Adsorbed Chiral Monolayer on Ferromagnets. *ACS Nano* **2021**, *15*, 5574−5579.
(24) Gutierrez, R.; Díaz, E.; Naaman, R.; Cuniberti, G. Spin-selective transport through helical molecular systems. *Phys. Rev. B: Condens. Matter Mater. Phys.* **2012**, *85*, 081404.
(25) Maslyuk, V. V.; Gutierrez, R.; Dianat, A.; Mujica, V.; Cuniberti, G. Enhanced Magnetoresistance in Chiral Molecular Junctions. *J. Phys. Chem. Lett.* **2018**, *9*, 5453−5459.
(26) Dalum, S.; Hedegård, P. Theory of Chiral Induced Spin Selectivity. *Nano Lett.* **2019**, *19*, 5253−5259.
(27) Shitade, A.; Minamitani, E. Geometric spin−orbit coupling and chirality-induced spin selectivity. *New J. Phys.* **2020**, *22*, 113023.
(28) Li, X.; Nan, J.; Pan, X. Chiral Induced Spin Selectivity as a Spontaneous Intertwined Order. *Phys. Rev. Lett.* **2020**, *125*, 263002.
(29) Utsumi, Y.; Entin-Wohlman, O.; Aharony, A. Spin selectivity through time-reversal symmetric helical junctions. *Phys. Rev. B* **2020**, *102*, 035445.
(30) Liu, Y.; Xiao, J.; Koo, J.; Yan, B. Chirality-driven topological electronic structure of DNA-like materials. *Nat. Mater.* **2021**, *20*, 638−644.
(31) Yang, X.; van der Wal, C. H.; van Wees, B. J. Spin-dependent electron transmission model for chiral molecules in mesoscopic devices. *Phys. Rev. B* **2019**, *99*, 024418.
(32) Yang, X.; van der Wal, C. H.; van Wees, B. J. Detecting Chirality in Two-Terminal Electronic Nanodevices. *Nano Lett.* **2020**, *20*, 6148−6154.
(33) Barron, L. D. True and false chirality and absolute asymmetric synthesis. *J. Am. Chem. Soc.* **1986**, *108*, 5539−5542.
(34) Rikken, G. L. J. A.; Raupach, E. Observation of magneto-chiral dichroism. *Nature* **1997**, *390*, 493−494.
(35) Tokura, Y.; Nagaosa, N. Nonreciprocal responses from non-centrosymmetric quantum materials. *Nat. Commun.* **2018**, *9*, 3740.
(36) Alpern, H.; Yavilberg, K.; Dvir, T.; Sukenik, N.; Klang, M.; Yochelis, S.; Cohen, H.; Grosfeld, E.; Steinberg, H.; Paltiel, Y.; Millo, O. Magnetic-related States and Order Parameter Induced in a Conventional Superconductor by Nonmagnetic Chiral Molecules. *Nano Lett.* **2019**, *19*, 5167−5175.
(37) Miwa, S.; Kondou, K.; Sakamoto, S.; Nihonyanagi, A.; Araoka, F.; Otani, Y.; Miyajima, D. Chirality-induced effective magnetic field in a phthalocyanine molecule. *Appl. Phys. Express* **2020**, *13*, 113001.
(38) Sukenik, N.; Tassinari, F.; Yochelis, S.; Millo, O.; Baczewski, L. T.; Paltiel, Y. Correlation between Ferromagnetic Layer Easy Axis and the Tilt Angle of Self Assembled Chiral Molecules. *Molecules* **2020**, *25*, 6036.
(39) Goren, N.; Yochelis, S.; Jung, G.; Paltiel, Y. Magnetic passivation using chiral molecules. *Appl. Phys. Lett.* **2021**, *118*, 172401.
(40) Fransson, J. Charge Redistribution and Spin Polarization Driven by Correlation Induced Electron Exchange in Chiral Molecules. *Nano Lett.* **2021**, *21*, 3026−3032.
(41) Baibich, M. N.; Broto, J. M.; Fert, A.; Van Dau, F. N.; Petroff, F.; Etienne, P.; Creuzet, G.; Friederich, A.; Chazelas, J. Giant magnetoresistance of (001)Fe/(001)Cr magnetic superlattices. *Phys. Rev. Lett.* **1988**, *61*, 2472−2475.
(42) Binasch, G.; Grünberg, P.; Saurenbach, F.; Zinn, W. Enhanced magnetoresistance in layered magnetic structures with antiferromagnetic interlayer exchange. *Phys. Rev. B: Condens. Matter Mater. Phys.* **1989**, *39*, 4828−4830.
(43) Camley, R. E.; Barnaś, J. Theory of giant magnetoresistance effects in magnetic layered structures with antiferromagnetic coupling. *Phys. Rev. Lett.* **1989**, *63*, 664−667.
(44) Fert, A. Nobel Lecture: Origin, development, and future of spintronics. *Rev. Mod. Phys.* **2008**, *80*, 1517−1530.
(45) Kudo, K.; Sumimoto, T.; Hiraga, K.; Kuniyoshi, S.; Tanaka, K. Evaluation of Electrical Properties of Evaporated Thin Films of Metal-Free, Copper and Lead Phthalocyanines by In-Situ Field Effect Measurements. *Jpn. J. Appl. Phys.* **1997**, *36*, 6994−6998.
(46) Barraud, C.; Seneor, P.; Mattana, R.; Fusil, S.; Bouzehouane, K.; Deranlot, C.; Graziosi, P.; Hueso, L.; Bergenti, I.; Dediu, V.; Petroff, F.; Fert, A. Unravelling the role of the interface for spin injection into organic semiconductors. *Nat. Phys.* **2010**, *6*, 615−620.
(47) Sanvito, S. The rise of spinterface science. *Nat. Phys.* **2010**, *6*, 562−564.
(48) Cinchetti, M.; Dediu, V. A.; Hueso, L. E. Activating the molecular spinterface. *Nat. Mater.* **2017**, *16*, 507−515.
(49) Isshiki, H.; Kondou, K.; Takizawa, S.; Shimose, K.; Kawabe, T.; Minamitani, E.; Yamaguchi, N.; Ishii, F.; Shiotari, A.; Sugimoto, Y.; Miwa, S.; Otani, Y. Realization of Spin-dependent Functionality by Covering a Metal Surface with a Single Layer of Molecules. *Nano Lett.* **2019**, *19*, 7119−7123.
(50) Hirayama, M.; Okugawa, R.; Ishibashi, S.; Murakami, S.; Miyake, T. Weyl Node and Spin Texture in Trigonal Tellurium and Selenium. *Phys. Rev. Lett.* **2015**, *114*, 206401.
(51) Furukawa, T.; Shimokawa, Y.; Kobayashi, K.; Itou, T. Observation of current-induced bulk magnetization in elemental tellurium. *Nat. Commun.* **2017**, *8*, 954.
(52) Sakano, M.; Hirayama, M.; Takahashi, T.; Akebi, S.; Nakayama, M.; Kuroda, K.; Taguchi, K.; Yoshikawa, T.; Miyamoto, K.; Okuda, T.; Ono, K.; Kumigashira, H.; Ideue, T.; Iwasa, Y.; Mitsuishi, N.; Ishizaka, K.; Shin, S.; Miyake, T.; Murakami, S.; Sasagawa, T.; Kondo, T. Radial Spin Texture in Elemental Tellurium with Chiral Crystal Structure. *Phys. Rev. Lett.* **2020**, *124*, 136404.
(53) Jedema, F. J.; Nijboer, M. S.; Filip, A. T.; van Wees, B. J. Spin injection and spin accumulation in all-metal mesoscopic spin valves. *Phys. Rev. B: Condens. Matter Mater. Phys.* **2003**, *67*, 085319.
(54) Dediu, V. A.; Hueso, L. E.; Bergenti, I.; Taliani, C. Spin routes in organic semiconductors. *Nat. Mater.* **2009**, *8*, 707−716.
(55) Warner, M.; Din, S.; Tupitsyn, I. S.; Morley, G. W.; Stoneham, A. M.; Gardener, J. A.; Wu, Z.; Fisher, A. J.; Heutz, S.; Kay, C. W. M.; Aeppli, G. Potential for spin-based information processing in a thin-film molecular semiconductor. *Nature* **2013**, *503*, 504−508.
(56) Atzori, M.; Tesi, L.; Morra, E.; Chiesa, M.; Sorace, L.; Sessoli, R. Room-Temperature Quantum Coherence and Rabi Oscillations in Vanadyl Phthalocyanine: Toward Multifunctional Molecular Spin Qubits. *J. Am. Chem. Soc.* **2016**, *138*, 2154−2157.
(57) Du, G.-F.; Fu, H.-H.; Wu, R. Vibration-enhanced spin-selective transport of electrons in the DNA double helix. *Phys. Rev. B* **2020**, *102*, 035431.
(58) Fransson, J. Vibrational origin of exchange splitting and "chiral-induced spin selectivity. *Phys. Rev. B* **2020**, *102*, 235416.

https://doi.org/10.1021/jacs.2c00496
J. Am. Chem. Soc. 2022, 144, 7302−7307